Icarus 355 (2021) 114130

Contents lists available at ScienceDirect

Icarus

journal homepage: www.elsevier.com/locate/icarus

The Eris/Dysnomia system I: The orbit of Dysnomia

B.J. Holler [a,*], W.M. Grundy [b], M.W. Buie [c], K.S. Noll [d]

[a] Space Telescope Science Institute, Baltimore, MD, USA
[b] Lowell Observatory, Flagstaff, AZ, USA
[c] Southwest Research Institute, Boulder, CO, USA
[d] Goddard Space Flight Center, Greenbelt, MD, USA

ARTICLE INFO

Keywords:
Kuiper belt
Trans-neptunian objects
Hubble space telescope observations
Orbit determination

ABSTRACT

We present new results on the Eris/Dysnomia system including analysis of new images from the WFC3 instrument on the Hubble Space Telescope (HST). Seven HST orbits were awarded to program 15171 in January and February 2018, with the intervals between observations selected to sample Dysnomia over a full orbital period. Using relative astrometry of Eris and Dysnomia, we computed a best-fit Keplerian orbit for Dysnomia. Based on the Keplerian fit, we find an orbital period of 15.785899±0.000050 days, which is in good agreement with recent work. We report a non-zero eccentricity of 0.0062 at the 6.2-σ level, despite an estimated eccentricity damping timescale of ≤17 Myr. Considering the volumes of both Eris and Dysnomia, the new system density was calculated to be 2.43±0.05 g cm^{-3}, a decrease of ~4% from the previous value of 2.52±0.05 g cm^{-3}. The new astrometric measurements were high enough precision to break the degeneracy of the orbit pole orientation, and indicate that Dysnomia orbits in a prograde manner. The obliquity of Dysnomia's orbit pole with respect to the plane of Eris' heliocentric orbit was calculated to be 78.29±0.65° and is in agreement with previous work; the next mutual events season will occur in 2239. The Keplerian orbit fit to all the data considered in this investigation can be excluded at the 6.3-σ level, but identifying the cause of the deviation was outside the scope of this work.

1. Introduction

The Kuiper Belt is a large collection of icy bodies found beyond Neptune (a>30.1 au) that are typically categorized into different dynamical populations based on their orbital characteristics (e.g., Gladman et al., 2008). Many of these Kuiper Belt Objects (KBOs) are thought to have formed in other regions of the outer solar system and were later emplaced on their current orbits during the era of planetary migration (e.g., Malhotra, 1993, 1995; Levison and Morbidelli, 2003; Gomes, 2003; Levison et al., 2008). Because of this, a majority of these populations contain an assortment of KBOs that span a wide range of sizes, colors, and compositions (e.g., Müller et al., 2010; Barucci et al., 2011; Brown, 2012; Hainaut et al., 2012; Lacerda et al., 2014; Bannister et al., 2020). Photometry and spectroscopy are the primary tools used to study the colors and surface compositions of KBOs, with thermal measurements providing diameter estimates, but the mass of a system can only be accurately calculated in binary or multiple systems. Binaries are thought to be quite common among certain Kuiper Belt populations (Noll et al., 2008; Noll et al., 2014; Fraser et al., 2017), but they are potentially challenging to detect and characterize due to a combination of small sizes, low albedos, large heliocentric distances, and small separations between components.

In the case of the dwarf planet (136199) Eris, the challenge in characterizing the orbit of its satellite Dysnomia is the system's extreme heliocentric distance (~96 au), resulting in a maximum angular separation of ~500 mas as seen from Earth. Only ground-based facilities equipped with adaptive optics (AO) and the Hubble Space Telescope (HST) are currently capable of reliably splitting the two components. The first published orbit for Dysnomia made use of AO data from Keck and HST data (Brown and Schaller, 2007), with a more recent orbit fit making use of the same data set plus previously unpublished HST data obtained in 2015 (Brown and Butler, 2018).

Brown and Schaller (2007) report two degenerate orbit solutions with different values for the semi-major axis of Dysnomia's orbit (37,430±140 and 37,370±150 km) and period (15.772±0.002 and 15.774±0.002 days) that cannot be distinguished from each other given their uncertainties. These two orbit solutions result in the same orbit pole obliquity (~78°) and two different but equally valid pole

* Corresponding author.
E-mail address: bholler@stsci.edu (B.J. Holler).

https://doi.org/10.1016/j.icarus.2020.114130
Received 16 November 2019; Received in revised form 10 September 2020; Accepted 28 September 2020
Available online 6 October 2020

orientations, corresponding to two dates for an orbit opening angle of 0°, 2239 and 2126, respectively. Brown and Butler (2018) report a semi-major axis of 37,460±80 km, which is in agreement with both solutions from Brown and Schaller (2007). However, they report a period of 15.78586±0.00008 days, which differs significantly from the previously reported periods (6.9-σ and 5.9-σ, respectively). The cause of this discrepancy, given that the two papers make use of the same data, with Brown and Butler (2018) only considering two additional data points, is not immediately clear. Brown and Butler (2018) do not report an orbit pole obliquity for comparison. Brown and Schaller (2007) initially reported eccentricities of <0.010 and <0.013 for the two degenerate orbit solutions, respectively. Brown and Butler (2018) further constrained the eccentricity to <0.004, suggesting that Dysnomia's orbit is possibly circular. The combination of previous results on the system mass (Brown and Schaller, 2007) and radii for Eris (Sicardy et al., 2011) and Dysnomia (Brown and Butler, 2018) suggest that the system is the most massive in the Kuiper Belt at $(1.66\pm0.02)\times10^{22}$ kg, and has a high estimated density of >2.5 g cm^{-3}.

In this work, we examined relative astrometry of Eris and Dysnomia in new HST imagery and report updated physical parameters for the system and updated orbital parameters for Dysnomia. We also report a pole orientation for Dysnomia's orbit and use this to evaluate the time of the next mutual events season, when Eris and Dysnomia will take turns eclipsing each other.

2. Observations

The imaging observations of Eris and Dysnomia used in this work were made between Dec. 3, 2005, and February 3, 2018, with NIRC2 at Keck and ACS/HRC, WFPC2/PC1, and WFC3/UVIS on the Hubble Space Telescope (HST). We summarize these observations below:

- Observations with NIRC2 on Keck were carried out as part of three different programs in August 2006. The relevant program IDs are C168OL (PI: M. Brown, 2006/08/20 & 2006/08/21), ENG (PI: nirc2eng, 2006/08/30), and K240OL (PI: Armandroff, 2006/08/30), and all data are available on the Keck Archive. Hundreds of 60-s exposures were taken with both the narrow and wide camera settings (plate scales of ~10 and ~40 mas/pixel, respectively). All observations were made with the laser guide star adaptive optics (LGS AO) system in order to separate Eris and Dysnomia. We used the published relative astrometry values from Brown and Schaller (2007) in this investigation; readers are referred to that paper and the associated supplementary material for more information on these data.
- HST GO programs 10545 and 10860 (PI: M. Brown) observed Eris and Dysnomia with the now-defunct High Resolution Channel (HRC) of the ACS instrument and the F606W filter. The plate scale of the HRC was ~27 mas/pixel and the PSF FWHM was ~50 mas at 0.60 μm (as reported in the ACS Instrument Handbook[1]). Program 10545 consisted of one HST orbit, referred to as a "visit," of Eris and Dysnomia with two nearly consecutive 300-s exposures on 2005/12/03. Program 10860 consisted of two visits, one with four 550-s exposures and the other with four 565-s exposures, on 2006/08/03. As with the Keck/NIRC2 data described above, the relative astrometry values used in this investigation were taken directly from Brown and Schaller (2007).
- HST GO program 11169 (PI: M. Brown) observed Eris and Dysnomia with the now decommissioned Wide Field and Planetary Camera 2 (WFPC2) on 2007/08/13. All 4 images were made in Visit 13 using Planetary Camera 1 (PC1). Two of the images were taken through the F606W filter with an exposure duration of 400 s; the other two images were 500 s and were taken through the F814W filter. The plate scale of WFPC2/PC1 was 46 mas/pixel. These data have not been previously published.
- HST GO program 13668 (PI: M. Buie) consisted of 2 nearly consecutive visits on both 2015/01/29 and 2015/02/01, for 4 total visits. Each visit consisted of one 80-s exposure and three 720-s exposures with WFC3/UVIS and the F350LP filter. The plate scale of WFC3/UVIS is 40 mas/pixel, with a PSF FWHM of ~72 mas at 0.35 μm (as reported in the WFC3 Instrument Handbook[2]). Astrometry of Eris and Dysnomia from these observations was previously published in Brown and Butler (2018); other observations from this program were used to identify the satellite of Makemake (Parker et al., 2016).
- HST GO program 15171 (PI: B. Holler) consisted of 7 visits made between 2018/01/01 and 2018/02/03. Each orbit consisted of four 348-s exposures and one 585-s exposure with WFC3/UVIS and the F606W filter. The PSF FWHM is ~67 mas at 0.60 μm (as reported in the WFC3 Instrument Handbook). These visits were originally planned to occur within one orbital period of Dysnomia (~16 days; Brown and Schaller, 2007). However, visit 3 (2018/01/03) was subject to a tracking failure, and so two of the 348-s exposures and the 585-s exposure were streaked and not used in this analysis. An additional visit was awarded on 2018/02/03 to compensate for these losses. Median images from all visits that were not subject to tracking errors are presented in Fig. 1 and show the relative positions of Eris and Dysnomia. These are new observations that have not been published previously.

The NIRC2, ACS/HRC, and WFPC2/PC1 data sets were considered together as one epoch (2005–2007) and the WFC3/UVIS data sets were considered as a separate epoch (2015–2018) for the following analysis. We refer to these as Epoch 1 and Epoch 2, respectively.

3. Analysis & results

Relative astrometry of Eris and Dysnomia for Epoch 1 was taken primarily from the supplementary information of Brown and Schaller (2007). The WFPC2 data from HST program 11169, included in Epoch 1 and presented here for the first time, were reduced with the WFPC2 pipeline, *calwp2* v2.5.5 (released April 17, 2009).[3] The *calwp2* pipeline performs an analog-to-digital correction, marks bad pixels, subtracts the bias image and dark frame, performs flat fielding, and applies a shutter shading correction. The relative positions of Eris and Dysnomia were then extracted from these processed images.

Relative astrometry of Eris and Dysnomia for Epoch 2 was performed on the reduced **_flt.** images retrieved from the MAST archive at STScI. Reduction of the raw images from HST programs 13668 and 15171 was handled by the WFC3 pipeline, *calwf3* v.3.4.1 (released April 10, 2017).[4] The *calwf3* pipeline flags bad pixels, performs bias correction, trims overscan regions, subtracts the contribution from the dark current, performs flat fielding, and normalizes the fluxes between the UVIS1 and UVIS2 detectors. The **_flt.** files do not undergo charge transfer efficiency (CTE) correction and no post-flash or cosmic ray corrections were implemented.

We used the method of PSF-fitting to calculate the positions of the Eris and Dysnomia PSFs to sub-pixel precision for the WFPC2 and WFC3 data. Tiny Tim version 7.5, the most recent version of the HST PSF-simulation software (e.g., Krist, 1993), was used to construct a grid of PSFs across the WFPC2 and WFC3 images. The PSF varies across the image due to distortion and the grid was sufficiently sampled to account for this effect. An initial guess for the position of Eris in the image was

[1] https://hst-docs.stsci.edu/display/ACSIHB/

[2] https://hst-docs.stsci.edu/display/WFC3IHB

[3] http://documents.stsci.edu/hst/wfpc2/documents/handbooks/dhb/wfpc2_dhb.pdf

[4] http://www.stsci.edu/files/live/sites/www/files/home/hst/instrumentation/wfc3/_documents/wfc3_dhb.pdf

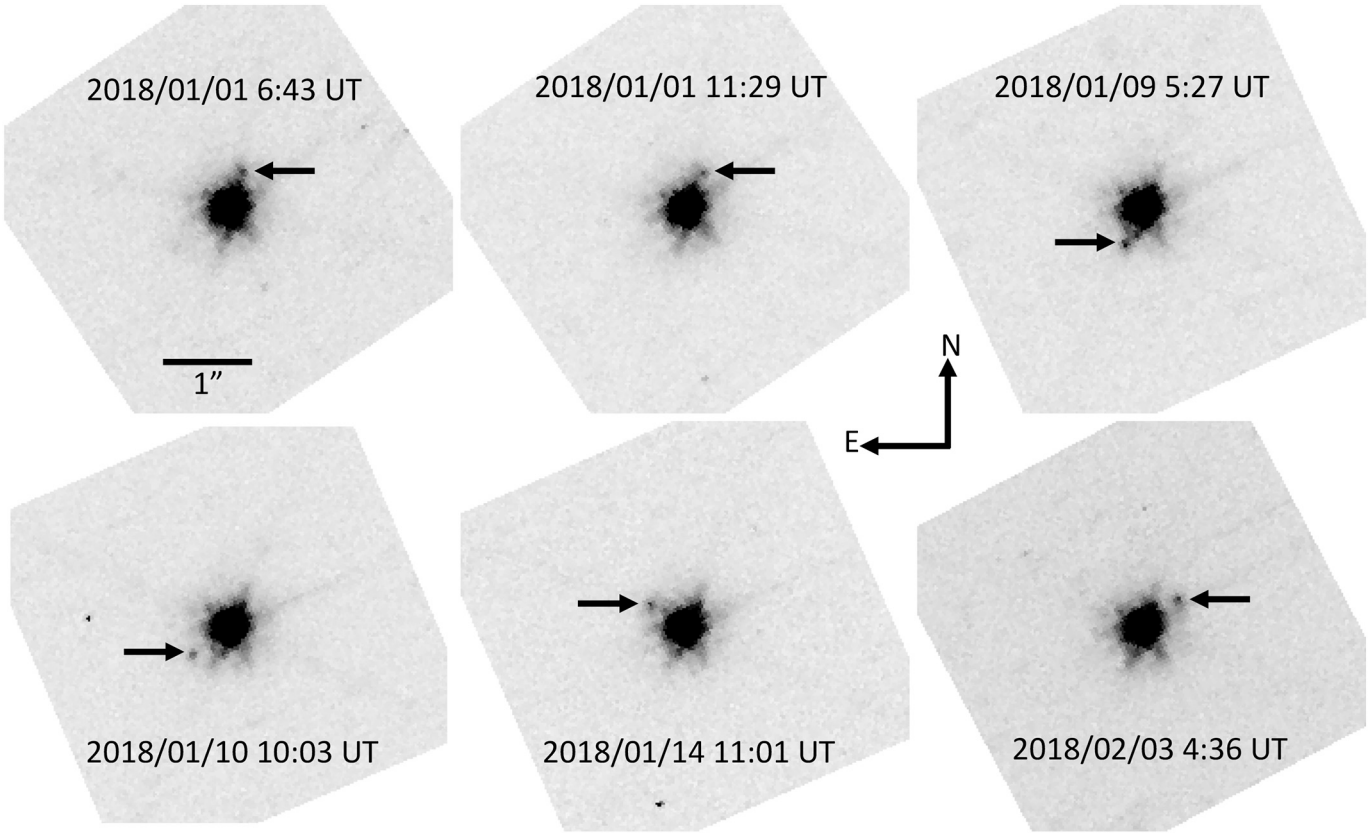

Fig. 1. Median of the four 348-s images from six visits of HST 15171 stretched to show both Eris and Dysnomia (denoted by the arrow). All images are shown using the same stretch and are rotated so that North is up and East is to the left. The median UT date and time are given for each image. Visits 1, 2, & 4 are along the top row; visits 5, 6, & 53 are along the bottom row. Visit 3 consisted of only two usable images so we do not present the median image here.

made to determine the nearest PSF on the grid for use in the PSF-fitting. KBOs are redder than the Sun, so we assumed the color index of a G5V star when creating the PSFs in Tiny Tim. Eris and Dysnomia were fit simultaneously using the *amoeba* IDL routine. The output centroid positions in detector coordinates were converted to right ascension and declination using the *xyad* IDL routine and the WCS solution provided in the FITS headers. Offsets of Dysnomia from Eris were calculated by subtracting the locations of the two objects. The right ascension and declination offsets and their corresponding 1-σ uncertainties are presented in Table 1. Uncertainties are reported as the standard deviation of the offsets from the individual images of each visit. An “error floor” was set at 2.26 mas, which was the average astrometric uncertainty in both right ascension and declination across all of the individual images from Epoch 2.

Table 1
Offsets of Dysnomia from Eris.

Mean UT date	RA offset (mas)	Dec offset (mas)	# of images
Epoch 1			
2007/08/13 2.04194	484.67±4.15	−178.10±2.68	4
Epoch 2			
2015/01/29 4.02507	−350.03±2.26	−226.03±2.26	4
2015/01/29 5.70083	−341.39±2.26	−229.13±2.26	4
2015/02/01 10.02840	+287.34±2.26	−328.08±2.26	4
2015/02/01 11.72611	+297.64±2.26	−323.68±2.26	4
2018/01/01 6.72108	−128.18±3.67	+363.10±2.26	5
2018/01/01 11.48714	−171.78±4.74	+362.48±2.26	5
2018/01/03 6.18291	−454.62±5.95	+226.35±3.61	2
2018/01/09 5.45492	+145.52±3.59	−366.50±2.74	5
2018/01/10 10.06408	+374.03±2.26	−296.19±2.32	5
2018/01/14 11.00769	+365.82±2.26	+221.95±2.26	5
2018/02/03 4.60881	−378.30±2.26	+277.49±2.26	5

The offsets of Dysnomia from Eris, along with geocentric distance and mean UT date, were used to compute the best-fit Keplerian orbit of Dysnomia around Eris shown in Fig. 2, with the residuals presented in Fig. 3. We fit the following set of parameters (see Table 2 for variable definitions): P, a, $e\cos\omega$, i, ε, Ω, $e\sin\omega$. The eccentricity, e, and argument of periapsis, ω, were extracted from $e\cos\omega$ and $e\sin\omega$. The eccentricity was calculated by adding $e\cos\omega$ and $e\sin\omega$ in quadrature, then the argument of periapsis, ω, was calculated using the eccentricity and either $e\cos\omega$ or $e\sin\omega$. The longitude of perihelion, ϖ, is defined as $\omega+\Omega$ and is reported in Table 2. The Keplerian orbits were computed for Epoch 1 and Epoch 2, separately, and Epochs 1 & 2 combined. The best-fit values, along with the χ^2 for each fit, are reported in Table 2. We adopt the values from the combined fit for the orbit of Dysnomia.

To calculate the uncertainties on the fitted parameters, we took each set of nominal parameters and varied each separately around the best-fit value, calculating the χ^2 for the orbit at each step. By varying only one parameter at a time the other parameters were forced to adjust. A parabola was then fit to χ^2 as a function of parameter value. The best-fit value from the orbit fit corresponded to the minimum χ^2 and asymmetric errors were found where the parabolic fit was equal to $\chi^2_{min}+1$. The uncertainties reported in Table 2 for the fitted elements are symmetric and are equal to the larger of the two asymmetric errors.

The derived parameters (and their uncertainties) in Table 2 were calculated using the fitted elements (and their uncertainties). The system mass, M_{sys}, was calculated from the period, P, and the semi-major axis, a, of Dysnomia using Newton’s version of Kepler’s Third Law. The standard gravitational parameter is simply the system mass multiplied by the gravitational constant. The equatorial coordinates of the Dysnomia orbit pole were calculated as $\alpha_{pole}=\Omega-90^\circ$ and $\delta_{pole}=90^\circ-i$. Due to the projection of the orbit onto the sky, there were two possible solutions for the orbit pole orientation. To break this mirror degeneracy,

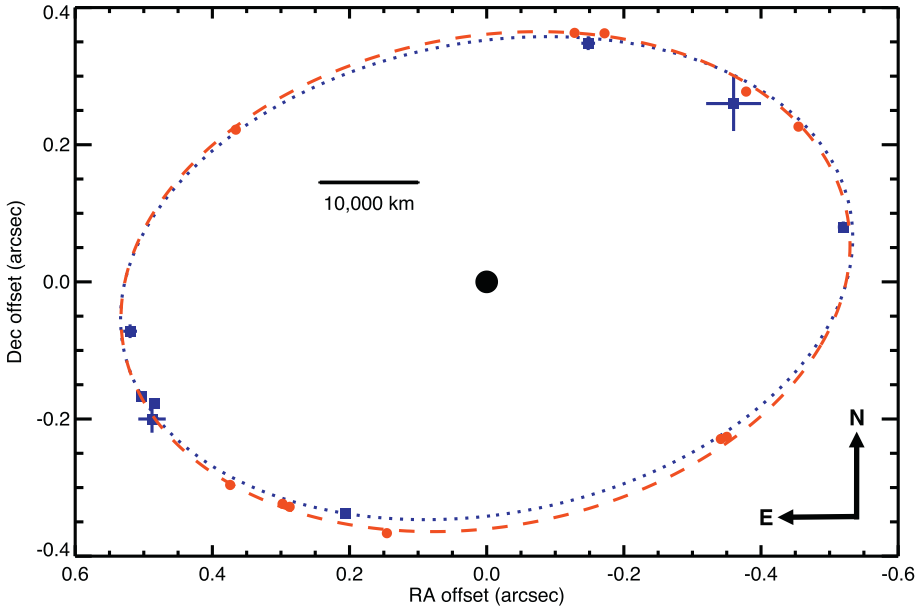

Fig. 2. Projected orbit of Dysnomia. North is up and East is to the left, in the direction of increasing right ascension. Eris is to-scale in the center (~30 mas diameter). The blue squares represent the positions of Dysnomia from Epoch 1. The red circles represent the positions of Dysnomia in Epoch 2. These symbols are not scaled to the estimated diameter of Dysnomia. Error bars are shown for all points but may be smaller than the symbol (see the supplementary material from Schaller and Brown (2007) for errors for Epoch 1 and Table 1 for Epoch 2). The blue dotted and red dashed lines represent the orbit fits to Epoch 1 and Epoch 2, respectively. (For interpretation of the references to color in this figure legend, the reader is referred to the web version of this article.)

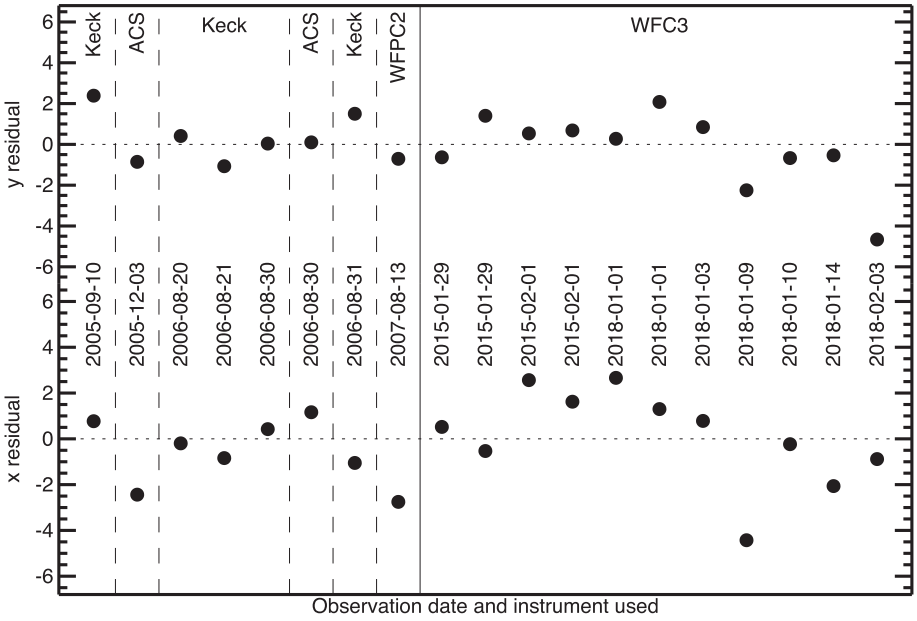

Fig. 3. Residuals in x (right ascension) and y (declination) for each observation. Units are number of 1-σ error bars. Each observation is labeled with the name of the instrument at the top of the plot and the UT date vertically in the middle. The solid grey line separates the Epoch 1 residuals (left side) from the Epoch 2 residuals (right side).

we evaluated the orbit solution for both cases and report the values for the orbit with the lower χ^2. This orbit pole position was then converted to ecliptic coordinates (λ_{pole}, β_{pole}) using standard spherical trigonometric formulae. The inclination to heliocentric orbit is the angle between Dysnomia's orbit pole and heliocentric orbital pole, and is also referred to as the obliquity of the orbit. It was calculated by taking the dot product between the Eris (λ_{Eris}=305.95°, β_{Eris}=45.99°) and Dysnomia orbit pole vectors. A value <90° indicates that Dysnomia's orbit is prograde.

The opening angle of Dysnomia's orbit between 1600 and 2500 C.E. was calculated using the orbit pole orientation determined in this work and a vector table of Cartesian positions from JPL/Horizons. The vector table for Eris was calculated with respect to the solar system barycenter in 1-year timesteps and included the light travel time correction. At each timestep, the x, y, and z positions of Eris defined the Eris-Sun vector (the distance from the center of the Sun to the solar system barycenter is negligible compared to the distance between Eris and the Sun). The orbit pole vector was defined in Cartesian coordinates using the orbit pole ecliptic latitude (β_{pole}) and longitude (λ_{pole}) from Table 2 and the equations below:

$$x = cos(\beta_{pole})sin(\lambda_{pole})$$
$$y = cos(\beta_{pole})sin(\lambda_{pole})$$
$$z = sin(\beta_{pole})$$

Taking the dot product of the Eris-Sun vector and Dysnomia's orbit pole vector yielded the value of the opening angle at that timestep. The orbit opening angle between 1600 and 2500 C.E. is presented in Fig. 4. The opening angle in early 2018 was 42°, and the next mutual events

Table 2
Orbital parameters and 1-σ uncertainties for epoch 2453979.0 JD.

Parameter		Epoch 1 (χ^2=18.9)	Epoch 2 (χ^2=69.6)	Combined (χ^2=107.6)
Fitted elements				
Period (days)	P	15.78674±0.00092	15.78645±0.00019	15.785899±0.000050
Semi-major axis (km)	a	37,636±216	37,332±94	37,273±64
Eccentricity	e	0.0156±0.0059	0.0035±0.0011	0.0062±0.0010
Inclination[a] (deg)	i	45.87±0.88	45.32±0.18	45.49±0.15
Mean longitude at epoch (deg)	ε	124.8±1.0	128.75±0.83	125.78±0.32
Longitude of ascending node[a] (deg)	Ω	126.2±1.1	126.16±0.32	126.17±0.26
Longitude of periapsis[a] (deg)	ϖ	28±20	322±24	307±12
Derived parameters				
Standard gravitational parameter (km^3 s^{-2})	μ	1131±19	1104±8	1099±6
System mass (10^{22} kg)	M_{sys}	1.695±0.029	1.654±0.012	1.6466±0.0085
Orbit pole right ascension[a] (deg)	α_{pole}	36.2±1.1	36.16±0.32	36.17±0.26
Orbit pole declination[a] (deg)	δ_{pole}	44.13±0.88	44.68±0.18	44.51±0.15
Orbit pole ecliptic longitude[b] (deg)	λ_{pole}	48.98±0.91	49.18±0.25	49.12±0.21
Orbit pole ecliptic latitude[b] (deg)	β_{pole}	28.05±0.87	28.57±0.19	28.41±0.16
Inclination to heliocentric orbit (deg)	i_{helio}	78.47±0.79	78.21±0.66	78.29±0.65
Next mutual events season (year)		2239	2239	2239

[a] Referenced to J2000 equatorial frame.
[b] Referenced to J2000 ecliptic frame.

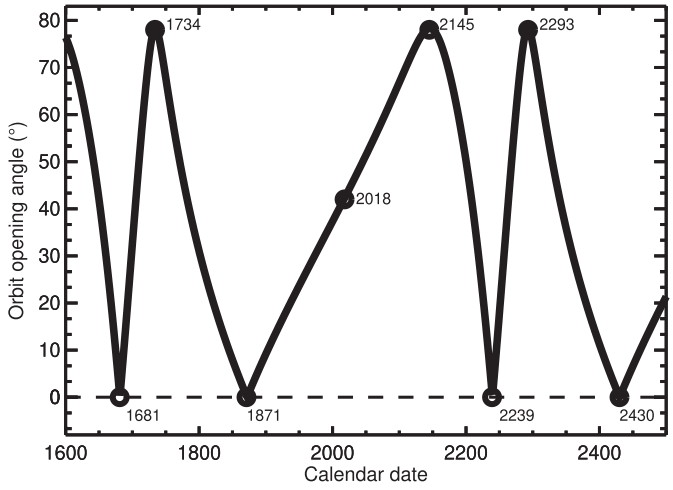

Fig. 4. Opening angle of Dysnomia's orbit as a function of date from 1600 to 2500 C.E; Eris' orbital period is approximately 558 Earth-years. The dates of maximum and minimum opening angles, as well as the most recent HST observations, 2018, are marked with open black circles. Mutual events occur when the opening angle reaches 0°, with the next instance in 2239. Assuming different values for β_{pole} and λ_{pole} (within the 1-σ error bars) changes the dates in this figure by no more than a few months and the opening angle by no more than ~0.20° on any given date.

season, when the opening angle reaches 0°, will occur in 2239.

4. Discussion

The orbit pole obliquity (78.29±0.65°) and the next mutual events season (2239 C.E.) determined in this work are consistent with the values calculated for Orbit 1 in Brown and Schaller (2007). The semi-major axis and system mass from the combined fit of this work are also in agreement with Orbit 1 (within 1-σ); the semi-major axis is in agreement with the value reported in Brown and Butler (2018) to within 2-σ. The period calculated in this work is in very good agreement with that reported in Brown and Butler (2018), with a difference of only ~3 s, but both values are inconsistent with those from Brown and Schaller (2007): 15.772±0.002 days for Orbit 1 and 15.774±0.002 days for Orbit 2. This is surprising given that the semi-major axis, period, and system mass are all related through Newton's version of Kepler's Third Law; however, the Brown and Schaller (2007) results for the period are clearly the outliers. Additionally, we note that Epoch 1 from this work, which made use of the same relative astrometry as Brown and Schaller (2007), plus an additional WFPC2 measurement, has a period which is in agreement with the fit to the Epoch 2 data, but not with the results of Brown and Schaller (2007).

The orbit angles (inclination and longitude of the ascending node) reported in both Brown and Schaller (2007) and Brown and Butler (2018) were referenced to the J2000 ecliptic frame, whereas those same values in this work were referenced to the J2000 equatorial frame (Table 2). After converting from the equatorial to the ecliptic frame, we found an inclination of 61.59±0.14° and a longitude of the ascending node of 139.12±0.22°. (We adopted the uncertainties from the equatorial frame for the parameters in the ecliptic frame.) We find that the inclination and longitude of the ascending node reported in this work agree with those for Orbit 1 from Brown and Schaller (2007), 61.3±0.7° and 139±1°, to within 1-σ and with those from Brown and Butler (2018), 61.1±0.3° and 139.6±0.2°, to within 2-σ.

We note a discrepancy in the RA offset between this work (Table 1) and Brown and Butler (2018) for 2015/02/01. Both investigations performed relative astrometry on images obtained as part of HST GO program 13668 (PI: M. Buie), and both investigations used a PSF-fitting method with PSFs generated by Tiny Tim. In this work, we report relative astrometry between Eris and Dysnomia for each visit of program 13668, whereas Brown and Butler (2018) reported a single RA offset and a single Dec offset for each UT date. Taking the average of our RA offsets and Dec offsets, in mas, for each UT date resulted in values of (−345.71±3.20, −227.58±3.20) for 2015/01/29 and (292.49±3.20, −325.88±3.20) for 2015/02/01. Comparison of these offsets to those in Brown and Butler (2018) resulted in differences, in mas, of (1.29±3.77, 1.58±3.35) for 2015/01/29 and (10.49±4.39, 0.88±3.77) for 2015/02/01. The offsets differ by less than 1-σ except for the RA offset on 2015/02/01, which shows a 2.4-σ difference. The difference is ~10.5 mas, which corresponds to about a quarter of a WFC3 pixel (40 mas/pixel plate scale) and about 15% of the PSF FWHM. This difference is therefore at the sub-pixel level and appears not to have produced a noticeable difference in the orbit fits between the two investigations. This discrepancy may simply be due to differences in the exact implementation of the PSF-fitting methods, such as the PSF color index and/or

the detector location at which the PSF was calculated.

The density of Eris was originally calculated to be 2.3±0.3 g cm^{-3} using the mass from Brown and Schaller (2007) and a radius of 1200±50 km determined directly from HST images (Brown et al., 2006). A stellar occultation by Eris in 2010 resulted in a more precise radius measurement of 1163±6 km, and the density was revised upwards to 2.52±0.05 g cm^{-3} (Sicardy et al., 2011). Brown and Butler (2018) reported a radius for Dysnomia of 350±57.5 km from thermal observations, which makes Dysnomia a large KBO in its own right and its contribution to the system mass therefore cannot be ignored. Using our more precise mass estimate of (1.6466±0.0085)×10^{22} kg, the Eris radius from Sicardy et al. (2011), and the Dysnomia radius from Brown and Butler (2018), we calculate a system density of 2.43±0.05 g cm^{-3}. The only reliable density measurement for a KBO satellite is for Charon, which has a density roughly 92% of Pluto's density (Stern et al., 2015); thus, it is not out of the question for Dysnomia to have a density which is comparable to Eris'. If Eris and Dysnomia have the same density, 2.43 g cm^{-3}, then Dysnomia accounts for ~3% of the total mass of the system. If Dysnomia has a much lower density than Eris (e.g., 0.8 g cm^{-3}) then it accounts for <1% of the system mass.

Orbit 1 from Brown and Schaller (2007) constrained Dysnomia's eccentricity to <0.010 and Brown and Butler (2018) further reduced this upper limit to <0.004. The eccentricity of the combined fit reported in this work, 0.0062±0.0010, is nominally in agreement with the Brown and Butler (2018) result, given the uncertainty reported in this work. The takeaway from the consistency between these two values is that Dysnomia's orbital eccentricity is exceedingly low. However, based on the uncertainty on the eccentricity measurement, we can report that the eccentricity is non-zero at the 6.2-σ level. We calculated the timescale for tidal circularization based on the nominal radius of Dysnomia (350 km; Brown and Butler, 2018) and two extreme values for Dysnomia's density (0.8 and 2.43 g cm^{-3}) using the equation from Goldreich and Soter (1966):

$$\tau_e = \frac{4}{63} Q \frac{M_D}{M_E} \left(\frac{a^3}{GM_E}\right)^{1/2} \left(\frac{a}{R_D}\right)^5.$$

In the above equation, Q is the unitless tidal dissipation factor (typically assumed to be 100 in the absence of additional information), M_D is the mass of Dysnomia, M_E is the mass of Eris and taken to be $M_{sys} - M_D$, a is the semi-major axis from the combined fit, and R_D is the radius of Dysnomia. For densities of Dysnomia of 0.8 and 2.43 g cm^{-3} we computed circularization timescales of ~5 Myr and ~17 Myr, respectively. Thus, regardless of Dysnomia's density, it should be on a perfectly circular orbit given its current semi-major axis.

The non-zero eccentricity could be real and a result of Dysnomia being in resonance with an unseen interior satellite. It is also possible that the eccentricity is not real and is instead a result of center-of-light versus center-of-body (CoL-CoB) offsets or systematic errors. A CoL-CoB effect is a result of large-scale, potentially high-contrast, albedo patterns and offsets a measured PSF centroid away from the actual center of the body because lower-albedo regions account for a smaller fraction of the PSF flux. The difference between Dysnomia's periapse and apoapse is 462±105 km, which is comparable to Dysnomia's radius (Brown and Butler, 2018). Considering the extreme case of an Iapetus-like Dysnomia with a large hemispherical contrast in visible albedo, the CoL-CoB offsets could be due to Dysnomia alone. However, Dysnomia's light curve amplitude is currently unconstrained and Iapetus' two-tone coloration appears to be a unique case made possible by Saturn's dust environment (e.g., Spencer and Denk, 2010). Additionally, Eris has a very low light curve amplitude that could be due to a uniform albedo distribution across the surface (e.g., Carraro et al., 2006; Duffard et al., 2008; Roe et al., 2008). If this is the case, Eris would not contribute appreciably to any CoL-CoB offsets. If instead we are viewing Eris nearly pole-on, the same regions of the surface would always be observed and would explain the low light curve amplitude, but would not preclude large-scale albedo features from creating a CoL-CoB offset. Thus, CoL-CoB offsets on both Eris and Dysnomia could combine to produce the non-zero eccentricity, but this is speculation and no firm evidence exists supporting this interpretation.

Another option is that the relative astrometric measurements are subject to systematic offsets, though it is unclear where they originated from. For instance, such offsets would not be due to the motion of Dysnomia during each 348-s exposure. At 96.6 au, one WFC3/UVIS pixel (40 mas) corresponds to ~2800 km and Dysnomia moves through 0.026% of its orbit, or ~30 km, in 348 s. Thus, Dysnomia's apparent motion shifts it, at most, ~1% of a pixel in each exposure, depending on the position along its projected orbit, and this is less than the uncertainty on the relative astrometry. It also seems unlikely that the offsets arise from the non-radially symmetric PSF of Eris affecting the PSF fit to Dysnomia. Not only should this be accounted for by fitting the PSFs to both objects simultaneously, but Dysnomia's PSF is not always affected by the same structures in Eris' PSF as it moves through different orbital longitudes. A somewhat more realistic possibility is that the color correction applied to the PSFs produced by Tiny Tim is not equally applicable to Eris and Dysnomia. We did not test different color corrections for the Tiny Tim PSFs so it is unclear if this would have a preferential and appreciable effect on the central position of either the Eris or Dysnomia PSF in every image. There is, of course, the possibility that a systematic effect is at play that we did not identify here. However, without of a well-supported and more believable alternate solution, we accept the non-zero eccentricity and 6.2-σ significance at face-value. Determining a physical process responsible for the non-zero eccentricity is outside the scope of this work.

The inclination values reported in this work are measured with respect to the J2000 equatorial frame (i.e., with respect to the Earth's equatorial plane). The fits provide no clues to the orientation of Dysnomia's orbit with respect to Eris' equatorial plane, they only provide a measurement of the orientation of the orbit pole with respect to Eris' heliocentric orbit. If the orbit pole and Eris' rotation pole were aligned, this would be evidence for a giant impact formation scenario for Dysnomia, and would enable the determination of seasons on Eris (as well as Dysnomia, assuming its rotation pole is parallel to the orbit and Eris rotation poles). However, there is no indication that this is the case, and estimates of the tidal damping timescale for the inclination are exceedingly long. The ratio of inclination and eccentricity damping timescales is given by Murray and Dermott (1999):

$$\frac{\tau_i}{\tau_e} = 7 \left(\frac{sini_0}{sin\varepsilon}\right)^2 \left(\frac{1}{cosi_0}\right),$$

where i_0 is the initial inclination of the system and ε is the angle between the tidal bulge and the line connecting the centers of the primary and secondary. It is related to the tidal dissipation factor, Q, by $\varepsilon = \frac{1}{2Q}$. Thus, for Q=100, ε=0.005 rad. For an initial inclination of 1°, the ratio of timescales is ~85, so for the optimistic case of an eccentricity damping timescale equal to 5 Myr, the inclination damping timescale is 425 Myr. This timescale increases quickly with initial inclination, so that for a modest initial inclination of only 3.27° the inclination damping timescale is comparable to the age of the solar system. If Dysnomia is a captured satellite, the initial inclination of its orbit could have been anywhere between 0° and 90° in order to match the constraint from this work that Dysnomia's orbit is prograde. The range of initial inclinations that result in aligned orbit and spin poles is small and there is no preference for an initial low-inclination orbit in this scenario, which suggests that if Dysnomia is a captured satellite, it would currently be on an inclined orbit with respect to Eris' equatorial plane.

The inclination damping timescale considered above only takes into account the effects of tidal bulges but not the oblateness of the primary. Even a modest oblateness of 1%, the upper limit for Eris determined by Sicardy et al. (2011), is enough to significantly alter a satellite's orbital evolution (e.g., Porter and Grundy, 2012). Therefore, additional

modeling work is needed to evaluate the evolution of Dysnomia's orbit, particularly the inclination with respect to Eris' equatorial plane. This investigation, which is outside the scope of the current work, would need to account for the effects of an oblate Eris on the damping of the orbit's inclination, since tidal damping alone is clearly negligible.

In Table 2, we note the high χ^2 for Epoch 2 and the combined orbit fits compared to the Epoch 1 orbit fit. This is easily explained by the difference in the size of the error bars between the two epochs (Fig. 2), and the smaller error bars for Epoch 2 weight the combined fit towards those points. However, the high χ^2 values also indicate that a Keplerian orbit is not the best-fit to the Epoch 2 measurements. In fact, a Keplerian orbit can be excluded at the 5.8-σ and 6.3-σ levels for the Epoch 2 and combined fits, respectively. Possible physical explanations for a non-Keplerian orbit include precession of Dysnomia's orbit due to an oblate Eris; a non-spherical Dysnomia; the presence of an additional, previously undetected satellite; or center-of-light versus center-of-body (CoL-CoB) offsets due to large-scale albedo patterns. Evaluation of the effects of a potential tidal bulge on Eris is the subject of future work and is outside the scope of this particular paper. A discussion of additional satellites around Eris was initially presented in Murray et al. (2018), with more detailed work currently in preparation.

5. Summary

We used relative astrometry from WFC3/HST images obtained in January and February 2018, combined with previously published and unpublished HST and Keck data, to compute a new orbit for Dysnomia and break the degeneracy in the orbit pole orientation. Highlights of the results and interpretations include:

- The calculation of a new orbital period for Dysnomia, 15.785899±0.000050 days, which agrees with the value from Brown and Butler (2018) to within ~3 s. Both investigations made use of the relative astrometry from Brown and Schaller (2007), yet the more recent periods are not in agreement with those reported in Brown and Schaller (2007) for Orbit 1 (15.772±0.002 days) or Orbit 2 (15.774±0.002 days). In other words, the older results are now outliers and have never been replicated, even when considering the same data set.
- An orbit pole obliquity of 78.29±0.65°, which agrees with Orbit 1 of Brown and Schaller (2007). The orbit opening angle in 2018 was 42° and the next mutual events season will be in 2239. Dysnomia's orbit is prograde.
- An update to the system density, 2.43±0.05 g cm^{-3}, which takes into account the system mass from the combined fit of (1.6466±0.0085)×10^{22} kg and volumes of both objects. If Eris and Dysnomia have the same density, Dysnomia accounts for ~3% of the system mass.
- A non-zero eccentricity for Dysnomia's orbit, 0.0062±0.0010, which is reported at a significance of 6.2-σ. Tidal circularization should occur within ~17 Myr even if Dysnomia's density is a third of the system density. Explanations for the non-zero eccentricity involving center-of-light versus center-of-body offsets or systematic errors are not favored; determining a physical cause of this non-zero eccentricity is outside the scope of this work.
- A Keplerian orbit for the combined fit that can be excluded at the 6.3-σ level, suggesting precession of Dysnomia's orbit due to the oblateness of Eris, an irregularly shaped Dysnomia, an unseen interior satellite, or center-of-light versus center-of-body offsets.

A possible future investigation related to this work is an evaluation of the non-Keplerian nature of Dysnomia's orbit in the context of an oblate Eris. The same investigation could provide clues to the inclination of Dysnomia's orbit with respect to Eris' equatorial plane, which could in turn enable an evaluation of short- and long-term seasonal cycles on Eris. A future paper will provide a detailed discussion on the search for a Pluto-like minor satellite system around Eris.

Declaration of Competing Interest

The authors declare no conflicts of interest.

Acknowledgements

The authors would like to thank the two anonymous reviewers for their helpful suggestions as well as Darin Ragozzine and Leslie Young for their constructive discussions. The authors appreciate the work of Crystal Mannfolk, Linda Dressel, and Kailash Sahu of STScI in helping to optimize the HST observations prior to execution. This work is based on observations made with the NASA/ESA Hubble Space Telescope, obtained from the data archive at the Space Telescope Science Institute. STScI is operated by the Association of Universities for Research in Astronomy, Inc., under NASA contract NAS 5-26555. Support for this work was provided by NASA through grant number GO-15171.001 from STScI.

References

Bannister, M.T., et al., 2020. Expanding Horizons: The Need for Direct Exploration of the Diverse Trans-Neptunian Solar System (submitted).
Barucci, M.A., et al., 2011. New insights on ices in Centaur and transneptunian populations. Icarus 214, 297–307.
Brown, M.E., 2012. The compositions of Kuiper Belt objects. Ann. Rev. Earth and Plan. Sci. 40, 467–494.
Brown, M.E., Butler, B.J., 2018. Medium-sized satellites of large Kuiper Belt objects. Astron. J. 156, 164.
Brown, M.E., Schaller, E.L., 2007. The mass of dwarf planet Eris. Science 316, 1585.
Brown, M.E., et al., 2006. Direct measurement of the size of 2003 UB313 from the Hubble Space Telescope. Astrophys. J. Lett. 643, L61–L63.
Carraro, G., et al., 2006. Time series photometry of the dwarf planet Eris (2003 UB313). A&A 460, L39–L42.
Duffard, R., et al., 2008. A study of photometric variations on the dwarf planet (136199) Eris. A&A 479, 877–881.
Fraser, W.C., et al., 2017. All planetesimals born near the Kuiper Belt formed as binaries. Nat. Astron. 1, 0088.
Gladman, B., Marsden, B.G., Vanlaerhoven, C., 2008. Nomenclature in the outer solar system. In: Barucci, M.A., Boehnhardt, H., Cruikshank, D.P., Morbidelli, A. (Eds.), The Solar System Beyond Neptune. University of Arizona Press, Tucson, pp. 43–57.
Goldreich, P., Soter, S., 1966. Q in the solar system. Icarus 5, 375–389.
Gomes, R.S., 2003. The origin of the Kuiper Belt high-inclination population. Icarus 161, 404–418.
Hainaut, O.R., Boehnhardt, H., Protopapa, S., 2012. Colours of minor bodies in the outer solar system. II. A statistical analysis revisited. A&A 546, A115.
Krist, J., 1993. Tiny Tim: An HST PSF simulator. In: Hanisch, R.J., Brissenden, R.J.V., Barnes, J. (Eds.), ASP Conf. Ser. 52, Astronomical Data Analysis Software and Systems II. ASP, San Francisco, p. 536.
Lacerda, P., et al., 2014. The albedo-color diversity of transneptunian objects. Astrophys. J. Lett. 793, L2.
Levison, H.F., Morbidelli, A., 2003. The formation of the Kuiper Belt by the outward transport of bodies during Neptune's migration. Nature 426, 419–421.
Levison, H.F., et al., 2008. Origin of the structure of the Kuiper Belt during a dynamical instability in the orbits of Uranus and Neptune. Icarus 196, 258–273.
Malhotra, R., 1993. The origin of Pluto's peculiar orbit. Nature 365, 819–821.
Malhotra, R., 1995. The origin of Pluto's orbit: implications for the solar system beyond Neptune. Astron. J. 110, 420–429.
Müller, T.G., et al., 2010. "TNOs are cool": a survey of the trans-Neptunian region. I. Results from the Herschel science demonstration phase (SDP). A&A 518, L146.
Murray, C.D., Dermott, S.F., 1999. Solar System Dynamics. Cambridge University Press.
Murray, K., Holler, B.J., Grundy, W., 2018. Search for a Pluto-like Satellite System Around Eris (AAS/DPS 50, #311.08).
Noll, K.S., et al., 2008. Evidence for two populations of classical transneptunian objects: the strong inclination dependence of classical binaries. Icarus 194, 758–768.
Noll, K.S., Parker, A.H., Grundy, W.M., 2014. All Bright Cold Classical KBOs are Binary (AAS/DPS 46, #507.05).
Parker, A.H., et al., 2016. Discovery of a Makemakean moon. Astrophys. J. Lett. 825, L9.
Porter, S.B., Grundy, W.M., 2012. KCTF evolution of trans-neptunian binaries: connecting formation to observation. Icarus 220, 947–957.
Roe, H.G., Pike, R.E., Brown, M.E., 2008. Tentative detection of the rotation of Eris. Icarus 198, 459–464.
Schaller, E.L., Brown, M.E., 2007. Volatile loss and retention on Kuiper Belt Objects. ApJ 659, L61–L64.
Sicardy, B., et al., 2011. A Pluto-like radius and a high albedo for the dwarf planet Eris from an occultation. Nature 478, 493–496.
Spencer, J.R., Denk, T., 2010. Formation of Iapetus' extreme albedo dichotomy by exogenically triggered thermal ice migration. Science 327, 432.
Stern, S.A., et al., 2015. The Pluto system: initial results from its exploration by New Horizons. Science 350, aad1815.